Polymer 49 (2008) 3295–3300

Contents lists available at ScienceDirect

Polymer

journal homepage: www.elsevier.com/locate/polymer

Markedly compressible behaviors of gellan hydrogels in a constrained geometry at ultraslow strain rates

Kenji Urayama [a,*], Yuta Taoka [a], Kunio Nakamura [b], Toshikazu Takigawa [a]

[a] Department of Materials Chemistry, Kyoto University, Kyoto 615-8510, Japan
[b] Department of Food Science, Rakuno Gakuen University, Hokkaido 069-8501, Japan

ARTICLE INFO

Article history:
Received 17 March 2008
Received in revised form 19 May 2008
Accepted 26 May 2008
Available online 6 June 2008

Keywords:
Gels
Fracture
Gellan

ABSTRACT

The fracture behaviors of gellan hydrogels under compression remarkably depend on the strain rate as well as the boundary conditions for lateral expansion. In the geometry with no constraint for lateral expansion (conventional uniaxial compression), the gels rupture at relatively small strains independently of the compression rates. In contrast, when the gels are compressed extremely slowly (at a strain rate of ca. 10^{-5} s^{-1}) in the geometry prohibiting the lateral expansion at their top and bottom surfaces, they are remarkably compressible down to 2% of the initial height without macroscopic fracture and they are accompanied by a large amount of water release. In such markedly compressed gels, many microscopic cracks are formed around the central layer, where strain concentration occurs due to the nonuniform deformation arising from the constrained geometry. In the highly compressible case, the formation of macroscopic cracks is prevented by the localization of microscopic cracks as well as the enhancement in mechanical toughness by a significant increase in polymer concentration due to water release.

1. Introduction

Gellan is a type of polysaccharide produced by the microorganism *Pseudomonas elodea*, and it has a linear structure with tetrasaccharide sequences comprising glucose, rhamnose, and glucuronic acid (Fig. 1) [1]. Aqueous solutions of gellan undergo gelation by cooling when the concentration of gellan is higher than the critical gelling concentration [2]. The sol–gel transition of gellan is thermoreversible, and the driving force for gelation is the random coil-to-helix transition [3]. The junctions are composed of double helix structures and/or their aggregates. Gellan gels are widely used in food industries, and their rheological properties have been investigated by many researchers [4–11]. In particular, the fracture behavior of gellan gels is an important issue because it is closely related to mastication. One of the present authors has discovered that the compression rate has a pronounced influence on the fracture behavior of gellan hydrogels [12]. At moderate and high compression rates, the gels exhibited brittle fracture at small strains of less than 30%. In contrast, at an extremely low compression speed (5 μm/min), the gels with an initial height of 10 mm were markedly compressible to 90% (i.e., 10% of the initial height) without any macroscopic fracture, but with a large amount of water leakage from the gels. Some groups [13,14] examined the large deformation behaviors of gellan hydrogels, but none of them observed such markedly compressible behaviors because of the moderate or high compression rates. For many gels, changes in the volume (swelling or shrinking) induced by imposed deformation have been reported. When deformation is applied to fully swollen gels in solvents, they change their volume due to the shift to the new swelling equilibrium state under the imposed field. The field-induced volume change has been studied for gels under tension [15,16], compression [17–19], shear flow [20], ultracentrifugal forces [21,22], and oscillating force [23]. The marked dependence of the fracture mode on the compression rates observed for gellan hydrogels may be one of the most dramatic phenomena caused by the field-induced volume change. The physical background for this characteristic fracture behavior, however, still remains unclear. Our further measurements have revealed that a finite vaporization of water from gellan hydrogels during slow compression and the boundary conditions at the top and bottom surfaces of the hydrogels significantly affect their fracture behavior. It must be noted that the interpretation of the phenomena regarding the fracture behavior of gellan hydrogels is not straightforward since the two abovementioned factors—the vaporization of water and the boundary conditions—were not taken into consideration in the first observation [12]. In this paper, we elucidate the mechanism of the markedly compressible behavior of gellan hydrogels on the basis of experiments in which water vaporization during compression is prohibited and the boundary conditions for lateral expansion are varied.

* Corresponding author.
E-mail address: urayama@rheogate.polym.kyoto-u.ac.jp (K. Urayama).

0032-3861/$ – see front matter © 2008 Elsevier Ltd. All rights reserved.
doi:10.1016/j.polymer.2008.05.045

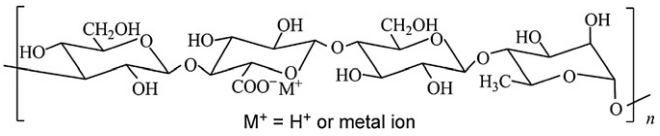

Fig. 1. Chemical structure of the repeating unit of gellan.

2. Experimental section

2.1. Materials and sample preparation

Powdered gellan was purchased from Wako Pure Chemical Ind., Japan and used without further purification. It was estimated by inductively coupled plasma–atomic emission spectrometry that 4300, 45,000, 3900, and 900 μg/g of Na^+, K^+, Ca^{2+}, and Mg^{2+}, respectively, were present in gellan.

The powdered gellan was dissolved in water at 75 °C for 2 h. The gellan concentration was 1.8 wt%. This concentration was chosen because a pronounced effect of the compression rate on the fracture behaviors was observed for the gels prepared with a concentration of around 2 wt%. The solution was poured into a mold and allowed to undergo gelation at 2 °C for 12 h. The resultant gels were removed from the mold and used for mechanical measurements. Cylindrical gels with a diameter of 26 mm and a height of 9 mm (Gel-L) were employed for most of the measurements. Smaller gels with a diameter of 13 mm and a height of 4.5 mm (Gel-S) were also used for comparison. The description of the data is for Gel-L, unless specified otherwise.

2.2. Compression measurements

The slow compression measurements were conducted using a UTM-4-100 (Toyo Baldwin) at constant crosshead speeds. The apparatus was modified so that the compression speed (v) could be reduced to 0.005 mm/min. RTM-250 (Orientec) was employed for the fast compression measurements ($v > 1$ mm/min). The crosshead speed was widely varied from 100 to 0.005 mm/min by using these two compression testers.

The compression tests were performed under the two boundary conditions (designated as C1 and C2) schematically shown in Fig. 2. The geometry C1 corresponds to the conventional uniaxial compression with no restriction for lateral expansion. Thin layers—with thickness of several hundred micrometers—of a highly viscous silicone oil (DMS-T41, Gelest Inc; 10,000 cSt) were placed on the top and bottom surfaces of the gels as lubricants in order to eliminate friction. The silicone oil layers did not diffuse within the time course of the compression measurements because of the high viscosity. The geometry C2 prohibits lateral expansion at the top and bottom surfaces of the gels during compression. Thin sandpapers with thicknesses of several hundred micrometers each were placed on the top and bottom surfaces of the gels. In all measurements, the gels were surrounded by liquid paraffin (non-solvent for the specimens) to prohibit water vaporization from the hydrogels during compression. We confirmed that no considerable leakage of water from the hydrogels surrounded by liquid paraffin occurred in the unloaded state, at least during the time taken for the compression measurements.

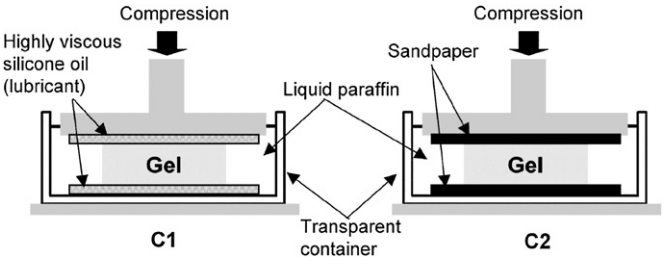

Fig. 2. Two geometries C1 and C2 with different boundary conditions employed in compression measurements.

The strains ε parallel ($\|$) and normal ($\perp$) to compression are defined as $\varepsilon_\| = -(h - h_0)/h_0$ and $\varepsilon_\perp = (d - d_0)/d_0$, where h and d are the height and diameter of the cylindrical gels, and the subscript 0 denotes the undeformed state. The condition C2 results in non-uniform deformation, in which case the profile of the compressed gels becomes appreciably convex, and the diameter has a maximal value at $h/2$ in the vertical direction. The maximum diameter at the central part was taken as d in the geometry C2 for the evaluation of $\varepsilon_\perp$. The compression process was recorded by a video camera, and the variations in the diameter and volume were evaluated from the profile of the compressed gels obtained by video analysis. Video analysis also confirmed that there was no appreciable slippage at the top and bottom surfaces of the gels compressed under C2.

3. Results

3.1. Stress–strain relations and water leakage at different compression rates

Fig. 3(a) shows the stress–strain curves in geometry C1 at various compression speeds (v). The stress (σ) is the nominal stress, i.e., the force divided by the cross-section in the undeformed state. The gels exhibit a macroscopic fracture under small or moderate strains ($\varepsilon_\| < 0.6$) in the entire v range examined. The stress–strain curves are almost independent of v.

The stress–strain curves in the geometry C2 at various v are illustrated in Fig. 3(b). The stress in the figure is the force divided by the cross-section of the top and bottom surfaces in the undeformed state. At a moderate v ($v > 0.1$ mm/min), the gels rupture under small strains ($\varepsilon_\| < 0.5$), in the same manner as the gels in geometry C1. A remarkable effect of the lateral expansion constraint is observed at slow compressions ($v < 0.05$ mm/min): the gels are markedly compressed to less than 10% of the initial height with no macroscopic fracture. In particular, at the slowest v (0.005 mm/min), the gel is compressible to only 2% of the initial height ($\varepsilon_\| = 0.98$). The appearance of such a highly compressed gel is shown in Fig. 4(b). In the case of $v = 0.05$ mm/min, the compressive force at $\varepsilon_\| \approx 0.9$ exceeded the capacity of the load cell, which precluded further compression.

The gels compressed at a moderate v (>0.1 mm/min) undergo macroscopic fracture independently of the boundary conditions. An appreciable difference in the crack patterns, however, is observed for such broken gels in geometries C1 and C2, as shown in Fig. 5. In C2, the broken gel shows noticeable cracks normal to the compression around the central part along with large cracks across from the top surface to the bottom; only the latter type of cracks is observed in C1.

When the gels are highly compressible, a large amount of water is expelled from the gels during compression. Fig. 6 shows the changes in the diameter and volume of the gels as a function of $\varepsilon_\|$ in C1 and C2. The strain $\varepsilon_\perp$ in C2 was evaluated from the maximum diameter at the central layer. The gel volume V in the figure is reduced by the volume V_0 before compression. The gels exhibiting macroscopic fracture show no significant change in volume before and after compression, i.e., $V/V_0 > 0.7$. In contrast, the highly compressed gels in C2 at $v = 0.05$ and 0.005 mm/min exhibit a large decrease in V during compression, i.e., a large amount of water is released from the gels. The high compression to $\varepsilon_\| = 0.8$ reduces the gel volume to ca. 20% of the initial volume.

3.2. Stress relaxation and water leakage at constant strains

To further elucidate the effects of the boundary conditions on the compression behaviors, we compare the stress relaxation and

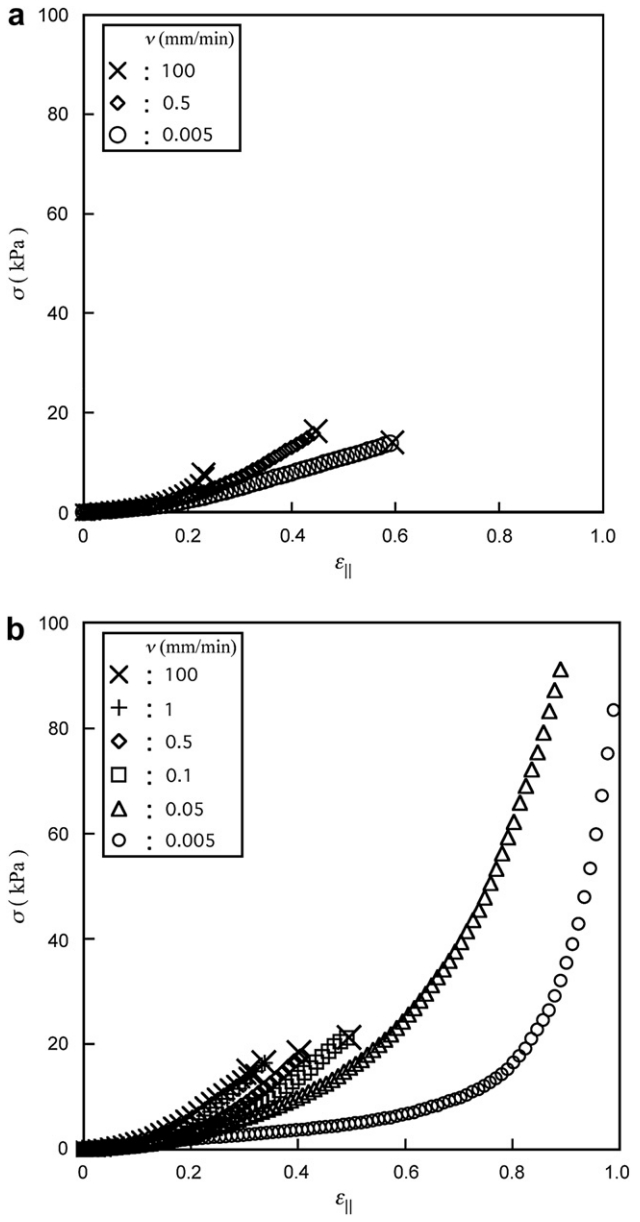

Fig. 3. Stress–strain curves of the gellan gels compressed at various crosshead speeds (ν) under (a) C1 and (b) C2 conditions. The crosses represent the strain at the macroscopic fracture. The gels compressed at $\nu = 0.05$ and 0.005 mm/min under the C2 condition exhibited no macroscopic fracture in the strain range examined. Further compression at $\nu = 0.05$ mm/min was precluded by the overload exceeding the capacity of the load cell.

volume variations at constant strains in geometries C1 and C2. The time dependencies of stress and volume after the imposition of a constant strain are shown in Fig 7(a) and (b), respectively. The stress and volume in the figures are normalized by the corresponding values σ_i and V_i at the time ($t = 0$) when the imposed strain $\varepsilon_{\|}$ reaches the destination strain ($\varepsilon_{\|} \approx 0.1$ or 0.3). The volume V_i was smaller than V_0 (volume before compression) because a small amount of water was released within the time required to reach the destination strain at $\nu = 0.5$ mm/min. Under a small constant strain ($\varepsilon_{\|} \approx 0.1$), the gel under C2 shows a considerably greater degree of stress relaxation (ca. 80%) than the gel under C1 (ca. 50%). At the corresponding strain, the gel under C1 exhibits no volume change ($V/V_i \approx 1$), while the volume of the gel under C2 slowly decreases by ca. 3%. Under a larger constant strain ($\varepsilon_{\|} = 0.3$), the stress under C2 reduces to almost zero, and the corresponding

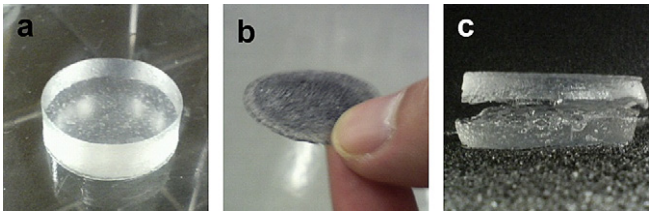

Fig. 4. (a) The gellan gel before compression. (b) The gel markedly compressed down to 2% of the initial height without macroscopic fracture at $\nu = 0.005$ mm/min under the C2 condition. The surface is blackish due to the color of the sandpaper used for the surface constraints. (c) The gel reswollen by water after high compression under C2. It should be noted that the gel splits around the central layer at $h/2$ in the vertical direction.

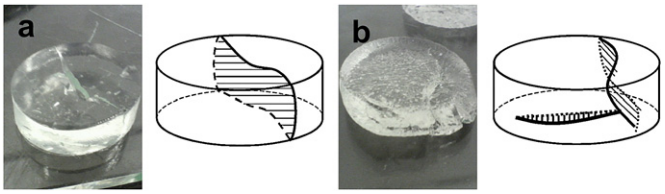

Fig. 5. Crack patterns of the broken gellan gels compressed at a rate of $\nu = 0.5$ mm/min under C1 (left) and C2 (right) conditions. Solid lines and shaded parts represent the visible and invisible parts of cracks, respectively.

volume reduction (ca. 7%) is considerably larger than that at $\varepsilon_{\|} = 0.11$. The magnitude of stress relaxation is closely correlated with that of water leakage.

Fig. 8 shows the effects of the gel dimension on the kinetics of stress relaxation and dimensional variation. A small gel (Gel-S), whose height and width are half to those of the gel in Fig. 7 (Gel-L), was employed for the comparison: the ratios of the height to the diameter of the two gels were identical; therefore, they could initially exhibit the same nonuniform deformation under C2. To facilitate the comparison of the kinetics, we use the normalized quantities A_σ and A_ε: $A_\sigma = (\sigma - \sigma_\infty)/(\sigma_0 - \sigma_\infty)$ and $A_\varepsilon = (\varepsilon_\perp - \varepsilon_{\perp\infty})/(\varepsilon_{\perp 0} - \varepsilon_{\perp\infty})$, where σ_∞ and $\varepsilon_{\perp\infty}$ are the equilibrium values. No appreciable difference in σ_∞ and $\varepsilon_{\perp\infty}$ was observed for the two gels. As is evident from the figure, the stress relaxation and dimensional change for Gel-S are faster than those for Gel-L. In addition, the stress relaxation proceeds more rapidly than the dimensional variation in each gel. The relaxation times τ_σ and τ_ε for σ and $\varepsilon_\perp$—which are defined as the time required to reach $A = 0.2$—are evaluated to be $\tau_\sigma = 5.0 \times 10^2$ and 2.5×10^3 s, $\tau_\varepsilon = 9.5 \times 10^3$ and 1.4×10^4 s for Gel-S and Gel-L, respectively.

4. Discussions

In this section, we consider the mechanism for the significant effects of the boundary conditions and the compression rate on the fracture behavior. A marked compression without macroscopic fracture and a large amount of water release were observed only in the sufficiently slow compressions under C2. While C1 leads to uniform uniaxial compression, C2 results in nonuniform compression that can be directly recognized from the convex outlines of the gels. The gels compressed under C2 have a maximal lateral expansion in the central layer at a height of $h/2$. The effect of such nonuniform distortion on the macroscopic fracture is also appreciable in the different crack patterns in the ruptured gels at moderately fast compressions under C1 and C2 (Fig. 5). The crack in the central layer specific to the macroscopic fracture under C2 is formed due to the strain concentration arising from nonuniform deformation.

When the compression rate is sufficiently slow, such strain concentration under C2 causes pronounced localization of the

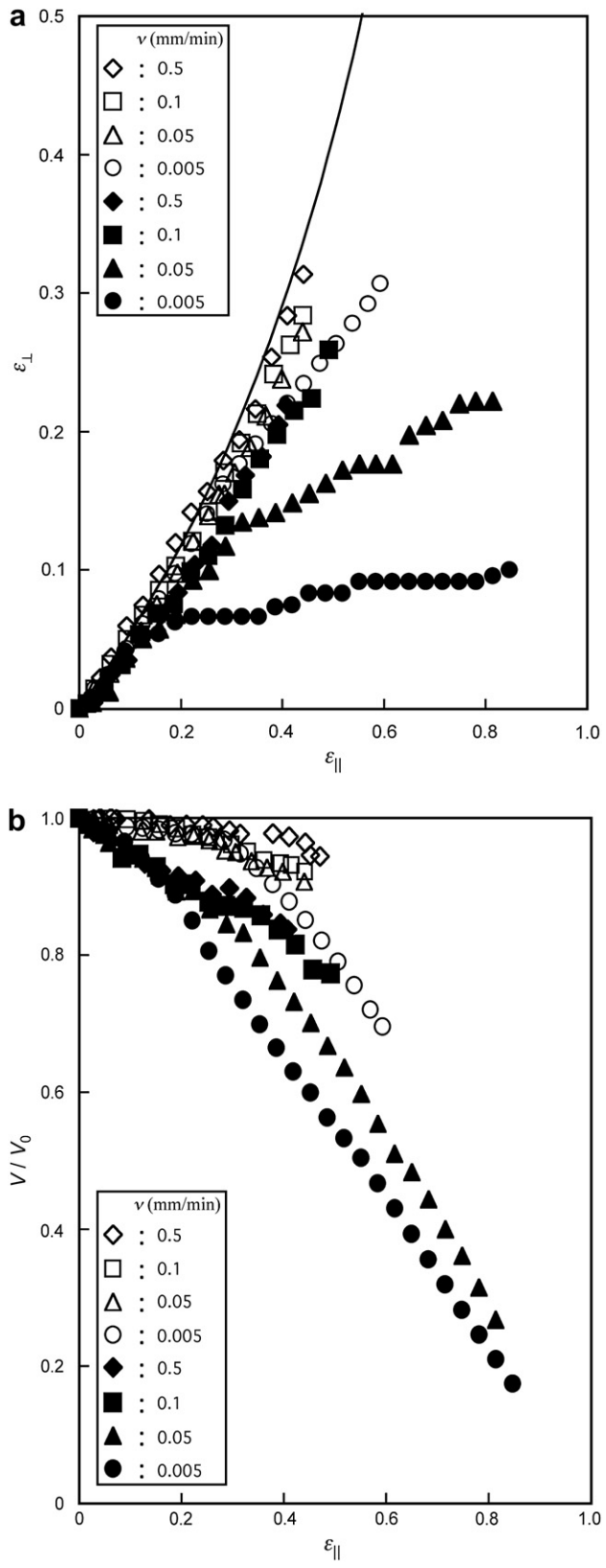

Fig. 6. (a) Diameter and (b) volume variations of gellan gels during compression at various crosshead speeds under C1 (open symbols) and C2 conditions (closed symbols). The solid line indicates the deformation with no volume change under C1.

microscopic fractures around the central layer. This is evident from the fact that when the highly compressed gels under C2 are allowed to reswell in water, they macroscopically split at the central part, as shown in Fig. 4(c). In the reswelling process, the swelling pressure is expected to assist the growth of microscopic cracks to macroscopic ones. This characteristic fracture on reswelling is a direct consequence of the presence of many microscopic fractures concentrated at the central layer. In other words, this observation indicates that the localization of the microscopic cracks at the central part plays an important role with regard to the highly compressible behavior. Almost no equilibrium stress at $\varepsilon_{\|}=0.3$ under C2 (Fig. 7(a)) suggests the formation of many microscopic fractures, even at relatively small strains.

Fig. 9 shows the schematics of the fracture behaviors under C1 and C2. In the sufficiently slow compression under C2, the microscopic cracks localized at the central part act as the paths for the outflow of water. A considerable increase in polymer concentration in the gels caused by the water release toughens the gels. This toughening prevents the microscopic cracks from developing into macroscopic cracks across the samples which lead to macroscopic failure. This mechanism of marked compression has a long and size-dependent characteristic time (τ_c). As observed in Fig. 8, the stress relaxation and volume variation become faster with a decrease in the gel diameter. This size dependence indicates that the water release process is involved in the mechanism of highly compressible behavior. The gels are markedly compressible when the compression rate is sufficiently lower than τ_c^{-1}. The characteristic time τ_c for Gel-L is roughly estimated to be ca. 1×10^4 s from $\tau_c \approx h_0/\nu_c$ using the critical condition for high compression ($\nu_c = 0.05$ mm/min). The time τ_c becomes shorter (or ν_c becomes larger) as the gel diameter decreases. The characteristic time for water diffusion across the gel (τ_w) is roughly evaluated to be 4×10^4 s for GEL-L from $\tau_w \approx (d/2)^2/(2D)$ where D ($\approx 2\times10^{-9}$ m^2/s) is the self-diffusion constant of water. The value of τ_w is in the same order of magnitude as τ_ε ($=1.4\times10^4$ s) obtained from the dimensional change at constant strain (Fig. 7) as well as τ_c evaluated from the critical compression rate (ν_c). This suggests that the water diffusion process is closely related to the markedly compressible behavior with water release. The kinetic aspect of highly compressible behavior, however, is not described solely by the water release process, because it results from the complicated combined effect of the processes of water release and microscopic fracture formation. Such a combined effect is also recognizable in Fig. 8 from the difference between the stress relaxation and the dimensional variation processes. In contrast, it is known that when the imposed strain is small enough (usually within the linear elasticity regime) to cause no microscopic fractures, the stress relaxation processes of poly(acrylamide) or poly(*N*-isopropylacrylamide) hydrogels agree with the kinetics of the induced swelling (i.e., $\tau_\sigma \approx \tau_\varepsilon$) [15,23]. In these cases, the stress relaxation is entirely attributable to the induced swelling.

Under C1 with no distribution of lateral expansion, the microscopic and/or macroscopic cracks can develop anywhere in the specimens. Since such cracks develop randomly, the paths for water flow have few chances to form. As is evident from Figs. 6(b) and 7(b), the amount of water release induced by compression under C1 is considerably smaller than that under C2. The gels under C1 exhibit the brittle fracture characteristic independently of ν because they have no microscopic mechanism to avoid the development of macroscopic fracture.

To the best of our knowledge, the gellan hydrogel is the only gel that exhibits markedly compressible behavior. Budtova and coworkers [19] observed a considerable water release ($V/V_0 \approx 0.6$) for chemically crosslinked poly(potassium acrylate-*co*-acrylamide) gels in a constrained geometry similar to C2 under slow compression (with a strain rate of ca. 10^{-3} s^{-1}); however, their gels underwent macroscopic fractures at small compressions ($\varepsilon_{\|} < 0.5$). We performed compression measurements for a chemically crosslinked poly(sodium acrylate-*co*-acrylicacid) hydrogel in the highly

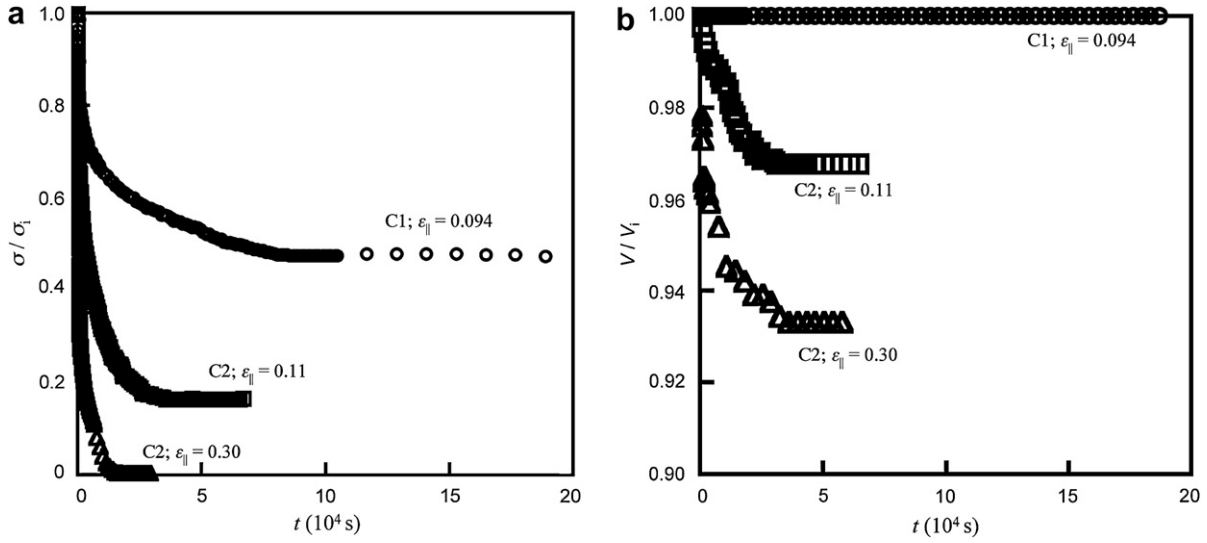

Fig. 7. (a) Stress relaxation and (b) volume variation of gellan gels at constant strains under C1 and C2 conditions.

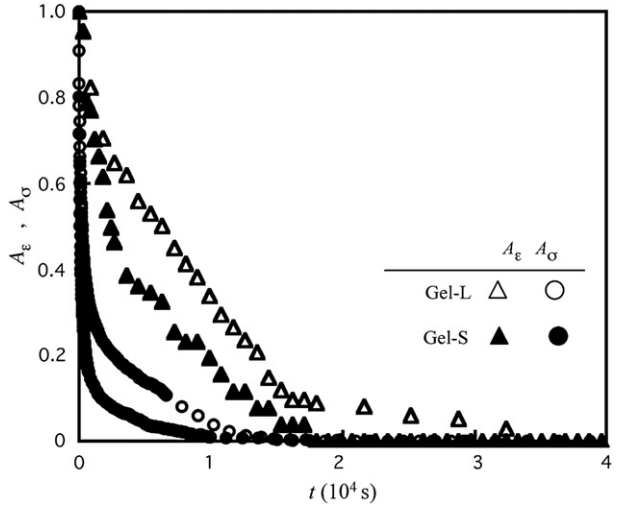

Fig. 8. Comparison of the time dependencies of stress relaxation and dimensional variation for Gel-L and Gel-S with different dimensions.

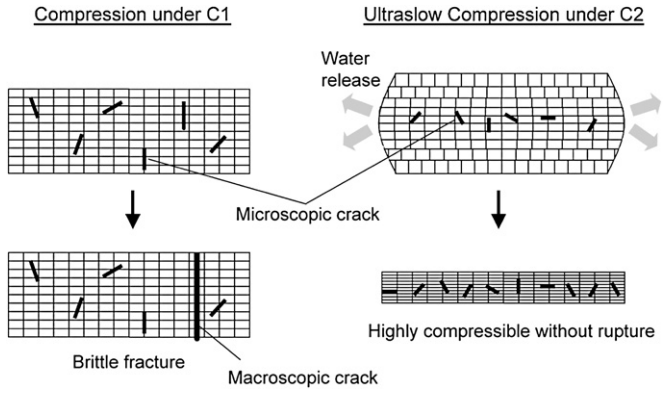

Fig. 9. (a) Brittle fracture under C1 condition and (b) markedly compressible behavior at extremely low compression rates under C2 condition.

swollen state (ca. 0.5 wt% in polymer concentration); in this state, its size was almost the same as that of Gel-L. A qualitatively similar behavior was observed for the compression-induced water release under C2, but the gel ruptured at small strains ($\varepsilon_{\|} < 0.4$), even when the compression rate was extremely low ($v = 0.005$ mm/min). It should be noted that the volume reduction (V/V_0) of the gel compressed extremely slowly at $\varepsilon_{\|} = 0.3$ (around the breaking point) was almost the same as that of the corresponding gellan gel. This implies that the compression rate was low enough to equilibrate the water release from the poly(sodium acrylate-*co*-acrylicacid) hydrogel. These results indicate that the markedly compressible behavior requires not only a large amount of water release but also a sufficient mechanical toughness of the gels. The mechanical toughness of gellan gels is enhanced by a significant increase in the network concentration due to water release during compression. The polymer concentration of the highly compressed gel ($\varepsilon_{\|} = 0.8$) corresponds to ca. 8 wt%; this is larger than the maximum concentration (ca. 3 wt%) achievable by the conventional dissolution of powdered gellan in hot water. The high compression effectively concentrates the gellan gels via water release, and the resultant gels with unusually high concentration are expected to possess sufficiently high toughness to be markedly compressed without macroscopic rupture.

5. Summary

Gellan hydrogels were markedly compressible down to a few percent of the initial height when they were compressed at extremely low rates (less than $10^{-5}\,s^{-1}$) in the geometry prohibiting the lateral expansion at their top and bottom surfaces. The marked compression was accompanied by a large amount of water release from the gels: a compressive strain of 80% reduced the gel volume to ca. 25% of the initial volume. Pronounced localization of microscopic cracks at the central layer with the maximum lateral expansion was observed. The enhancement in the mechanical toughness by a significant increase in polymer concentration arising from water release as well as the localization of microscopic cracks in the central layer prevented the development of a macroscopic fracture. The boundary conditions and strain rate had pronounced effects on the fracture behaviors. The compression in the unconstrained geometry for lateral expansion (corresponding to conventional uniaxial compression) resulted in macroscopic fracture at small strains without significant water leakage, independent of the strain rate. The compression rates that were higher than the critical rate also caused macroscopic fractures, even in the constrained geometry.

Acknowledgments

This work was partly supported by the Grant-in-Aid on Priority Area "Soft Matter Physics" (No. 19031014). This research was also supported in part by the Global COE Program "International Center for Integrated Research and Advanced Education in Materials Science" (No. B-09) of the Ministry of Education, Culture, Sports, Science and Technology (MEXT) of Japan, administrated by the Japan Society for the Promotion of Science.

References

[1] Jansson PE, Lindberg B, Lindquist U, Carlo DJ. Carbohydr Res 1983;118:157–71.
[2] Nishinari K, editor. Physical chemistry and industrial application of gellan gum. Berlin: Springer; 1999.
[3] Kanesaka S, Watanabe T, Matsukawa S. Biomacromolecules 2004;5:863–8.
[4] Nussininovitch A, Kaletunc G, Normand MD, Peleg M. J Texture Stud 1990;21:427–38.
[5] Tang JM, Lelievre J, Tung MA, Zeng YY. J Food Sci 1994;59:216–20.
[6] Hamann DD, Zhang JH, Daubert CR, Foegeding EA, Diehl KC. J Texture Stud 2006;37:620–39.
[7] Gambareli FR, Serra MD, Pereira LJ, Gaviao MB. J Texture Stud 2007;38:2–20.
[8] Gunning AP, Kirby AR, Ridout MJ, Brownsey GJ, Morris VJ. Macromolecules 1996;29:6791–6.
[9] Miyoshi E, Takaya T, Nishinari K. Carbohydr Polym 1996;36:109–20.
[10] Nakamura K, Tanaka Y, Sakurai M. Carbohydr Polym 1996;30:101–8.
[11] Nickerson MT, Paulson AT, Speers RA. Food Hydrocolloids 2004;18:783–94.
[12] Nakamura K, Shinoda E, Tokita M. Food Hydrocolloids 2001;15:247–52.
[13] Tang J, Tung MA, Lelievre J, Zeng Y. J Food Eng 1997;31:511–29.
[14] Kawai S, Nitta Y, Nishinari K. J Appl Phys 2007;102:043507.
[15] Takigawa T, Urayama K, Morino Y, Masuda T. Polym J 1993;25:929–37.
[16] Chiarelli P, Basser PJ, Derossi D, Goldstein S. Biorheology 1992;29:383–98.
[17] Hecht AM, Geissler E. J Chem Phys 1980;73:4077–80.
[18] Milimouk I, Hecht AM, Beysens D, Geissler E. Polymer 2001;42:487.
[19] Vervoort S, Patlazhan S, Weyts J, Budtova T. Polymer 2005;46:121–7.
[20] Zanina A, Budtova T. Macromolecules 2002;35:1973–5.
[21] Urayama K, Okada S, Nosaka S, Watanabe H, Takigawa T. J Chem Phys 2005;122:024906.
[22] Nosaka S, Okada S, Takayama Y, Urayama K, Watanabe H, Takigawa T. Polymer 2005;46:12607–11.
[23] Nosaka S, Urayama K, Takigawa T. Polym J 2005;37:694–9.